RSC Advances

PAPER

View Article Online
View Journal | View Issue

Cite this: *RSC Adv.*, 2018, **8**, 12292

Bimetallic carbide of Co_3W_3C enhanced non-noble-metal catalysts with high activity and stability for acidic oxygen reduction reaction

Bolin Li, Jianmin Zhou, Ling Zhang and Zesheng Li *

Received 20th January 2018
Accepted 25th March 2018

DOI: 10.1039/c8ra00602d

rsc.li/rsc-advances

A bimetallic carbide enhanced nitrogen/phosphor co-doped graphite nanocomposite (Co_3W_3C/NPG) is proposed for the first time as a highly active and stable non-noble-metal catalyst for the oxygen reduction reaction (ORR). The newly multi-component Co_3W_3C/NPG catalysts presented a high on-set potential of 0.92 V and little decreased half-wave potential of 5 mV after 8000 cycles in the O_2-saturated 0.1 M $HClO_4$ electrolyte. The electron transfer number was calculated to be above 3.9 before and after 8000 cycles, indicating that the Co_3W_3C/NPG catalyst behaves as a steady 4e oxygen reductant in acidic medium.

1. Introduction

Cathodic oxygen reduction reaction (ORR) is an active area of research due to its crucial role in electrochemical energy conversion for proton exchange membrane fuel cells (PEMFCs).[1] However, the dependence on expensive Pt-based ORR catalysts in PEMFCs remains a major obstacle for the widespread deployment of this technology.[2] One solution to overcome this predicament is to reduce the Pt usage veritably by introducing non-noble-metal catalysts at the oxygen-reducing cathode.[3] Metal/nitrogen/carbon (Me/N/C) catalysts obtained by the heat treatment of Fe and/or Co precursors as well as nitrogen and carbon precursors are one of the most promising non-noble-metal catalysts.[4] Though such highly active Me/N/C catalysts may approach to the target activity for PEMFC application, their electrochemical stability under the acidic and oxidizing environment of ORR still remains a great challenge.[5]

Carbide-based electrocatalysts have been intensively studied because of their electrocatalytic synergistic effect and their Pt-like behavior for chemical catalysis.[6] It is widely reported that tungsten carbides-promoted noble-metal electrocatalysts are highly active for both the oxygen reduction and alcohol oxidation reactions in fuel cells.[7] The origin of synergistic effect can be explained by the strong electron-donating effect generated by the WC.[8] Although carbide-promoted noble-metal catalysts are widely reported, the carbide-promoted non-noble-metal catalysts are rarely reported. On the other hand, phosphorus, an element of the nitrogen group, has been approved catalytically active for ORR in P-doped graphite.[9] Although the high activity of P doped carbon for ORR has been recently investigated in alkaline medium,[10] to our knowledge, there is little report on the high-performance N and P co-doped carbon and carbide materials for ORR in acidic medium.[11]

Herein, we synthesized a novel bimetallic carbide enhanced N and P co-doped graphite nanocomposite (Co_3W_3C/NPG) and we examined its electrochemical properties. The results demonstrate that this hybrid electrocatalyst shows high catalytic activity and long-term stability for ORR in acidic medium. The N and P co-doped graphite (NPG, in form of Co/N/P/C) is a more active non-noble-metal catalyst than N-doped graphite (NG, in form of Co/N/C) in 0.1 M $HClO_4$ electrolyte. The Co_3W_3C/NPG catalyst shows much higher activity and stability than the NPG catalyst in 0.1 M $HClO_4$ electrolyte. Our results suggest that bimetallic carbide of Co_3W_3C plays an important role in the significantly enhanced performances of the non-noble-metal catalyst: (i) the Co element in the carbide endows with a higher stability of the Co/N/P/C active component; (ii) the W-based carbide actually is a synergistic component that boosts the activity of the hybrid catalyst system.

2. Experimental

2.1. Materials synthesis

The ion-exchange resins are polymers composed of high molecular weight polyelectrolyte that can exchange their mobile ions with targeted ions from the surrounding medium. The ion exchange is a reversible chemical reaction wherein an ion from solution is exchanged by a similarly charged ion attached to an immobile solid particle. During the ion exchange process, ion diffuses from the solution to the surface of resin, further diffuses into the resin to ionic groups, and exchanges with them. The bimetallic carbide enhanced nitrogen/phosphor co-doped graphite (Co_3W_3C/NPG) nanocomposites were

Technology Research Center for Petrochemical Resource Cleaner Utilization of Guangdong Province, School of Chemical Engineering, Guangdong University of Petrochemical Technology, Maoming, 525000, P. R. China. E-mail: lzs212@163.com; Tel: +86 18718541956

synthesized according to a newly-developed ion-exchange procedure, by introducing an amidogen-functionalized ion-exchange resin as the initial precursor (see structure model below). The nitrogen source is from the amidogen group in the ion-exchange resin. The phosphor source, cobalt source and tungsten source are successively introduced by the ion exchange process. In a typical preparation, 50 g of macroporous acrylic-type anion-exchange resin (D314) was first impregnated with 1000 mL of 0.1 M ammonium metatungstate hydrate ($(NH_4)_6H_2W_{12}O_{40}$) and sodium hexanitrocobaltate ($Na_3Co(NO_2)_6$) solution. The resulting resin complex (Co and W contained anions) was then impregnated again with 100 mL of 0.05 M ammonium phosphate ($(NH_4)_3PO_4$) solution. The resulting resin complex (Co, W and P contained anions) was dried at 80 °C for 12 h, and then carbonization and graphitization were performed in a tube furnace at 1200 °C for 2 h at a heating rate of 10 °C min^{-1} under a pure Ar flow. After the sample was cooled to room temperature, the resulting product was shattered into fine powder by mechanical milling. For the purpose of comparison, NPG sample (without the tungsten source) NG sample (without the phosphor source and tungsten source) were also synthesized by the same ion exchange-assisted heat treatment strategy. All these samples have equivalent nitrogen doping and the same addition of cobalt or phosphor.

2.2. Materials characterizations

The X-ray diffraction (XRD) measurements were carried out on a D/Max-IIIA (Rigaku Co., Japan) employing Cu Ka ($\lambda = 0.15406$ nm) as the radiation source at 40 kV and 40 mA with a scanning rate of 8° min^{-1}. The morphology of the samples was observed by scanning electron microscopy (SEM) (FEI Quanta 200 FEG). The transmission electron microscopy (TEM) investigations were performed on a JEOL JEM-2010 operating at 200 kV. The X-ray photoelectron spectroscopy (XPS) measurements were carried out on an XPS apparatus (ESCALAB 250).

2.3. Electrochemical performances

The catalytic activity of the electrocatalysts for the ORR were evaluated by using a rotating ring-disk electrode (RRDE) with a biopotentiostat (AFCBP1E, Pine Instrument Co., USA) in a thermostat-controlled standard cell at 258C. A RRDE with a Pt ring (inner/outer-ring diameter: 6.25/7.92 mm) and a glassy carbon disk (diameter: 5.61 mm) was used as the working electrode. A home-made reversible hydrogen electrode (RHE) was used as the reference electrode and platinum foil (1.0×1.0 cm^2) was used as the counter electrode. The thin-layer working electrode was prepared as follows: a mixture of the electrocatalyst (5.0 mg), EtOH (1.8 mL), and Nafion suspension (0.2 mL, 0.5 wt%, DuPont, USA) was placed in an ultrasound bath for 30 min to obtain a well-dispersed electrocatalyst ink. The electrocatalyst ink was then quantitatively transferred onto the surface of the RRDE by using a microsyringe and dried under an IR lamp to obtain a thin-layer electrocatalyst. The electrocatalyst loadings were maintained at 200 μg cm^2 throughout this study. The ORR activities of the electrocatalysts were measured in an oxygen-saturated 0.1 M $HClO_4$ solution with a scan rate of 5 mV s^{-1} for the disk whilst keeping the ring potential at 1.2 V (*versus* RHE). The CV cycling (8000 CV cycles) of the electrocatalysts were measured at 50 mV s^{-1} between 0.0–1.1 V (*versus* RHE) in O_2-saturated 0.1 M $HClO_4$ solution.

3. Results and discussion

The crystallographic structures of the samples including NG (Co/N/C), NPG (Co/N/P/C) and Co_3W_3C/NPG are examined by X-ray powder diffraction (XRD), as shown in Fig. 1. The as-prepared NG sample contains graphite and Co (PDF# 01-1255) components, and the NPG sample contains graphite and Co_2P (PDF# 32-0306) components. Co species serve as the catalyst media for the graphitization of carbon precursor. Comparison with the NPG sample indicates that distinct diffraction peak of Co_3W_3C (PDF# 27-1125), besides the graphite and Co_2P phases, can be observed for the Co_3W_3C/NPG sample. The result indicates that bimetallic carbide from Co, W and C elements has been successfully achieved by present straightforward ion exchange-assisted heat treatment synthetic strategy.

The analysis of X-ray photoelectron spectroscopy (XPS) validates the successful incorporation of nitrogen and phosphorus atoms into the graphite structures (see Fig. 2 for evidence). The N1s spectrum in Fig. 2 (a) shows that one dominant type of N is present at 401.5 eV, corresponding to the "graphitic" N (*i.e.* N atoms linked with three C atoms at the same) in graphene. In addition, the P2p spectrum in Fig. 2 (b) indicates that oxidized P (133.2 eV) and graphitic P (130.5 eV) coexist in the sample. The surface contents of nitrogen and phosphorus for the sample are 3.36% and 1.97% in atomic ratio.

Fig. 3 shows the SEM-EDS elemental mapping images of C, Co, W, O and P from the individual Co_3W_3C/NPG block. It is found that the five elements are homogeneously distributed corresponding to the SEM image (Fig. 3(a)). Fig. 3(b) further reveals the EDS spectroscopy (the inset shows the element content) of the sample. The weight percentage of C, Co, W, O and P are 60.70, 4.71, 19.19, 4.09 and 0.81, respectively. And the atomic percentage of C, Co, W, O and P are 88.90, 1.84, 1.14, 4.49 and 0.46, respectively. The N is cannot be detected by EDS and Cu is from the Cu-based sample platform.

The morphology and microstructure of the Co_3W_3C/NPG sample are examined by the transmission electron microscopy (TEM) (see Fig. 4). From the general TEM images (Fig. 4(a) and (b)), it can be observed that multitudinous nanoparticles of about 20 nm size are loaded on the two-dimensional carbon structures. A high-resolution TEM image (Fig. 4(c)) shows visible lattice planes of the nanocrystal, showing two different spacing of approximately 0.63 and 0.25 nm, corresponding to the (111) and (311) planes of Co_3W_3C, respectively. The graphite (002)-oriented Inverse Fourier Transform (IFT) image based on Fig. 4(c) illustrates the graphite with 1–5 layer graphene-like structures ($d_{(002)} = 0.34$ nm) which surrounds the Co_3W_3C nanocrystals (see Fig. 4(d)). The sp^2-bonded graphite carbon distributing on the two-dimensional carbon structures guarantee a high electrical conductivity of the resultant nanomaterials. More importantly, these graphite carbons provide

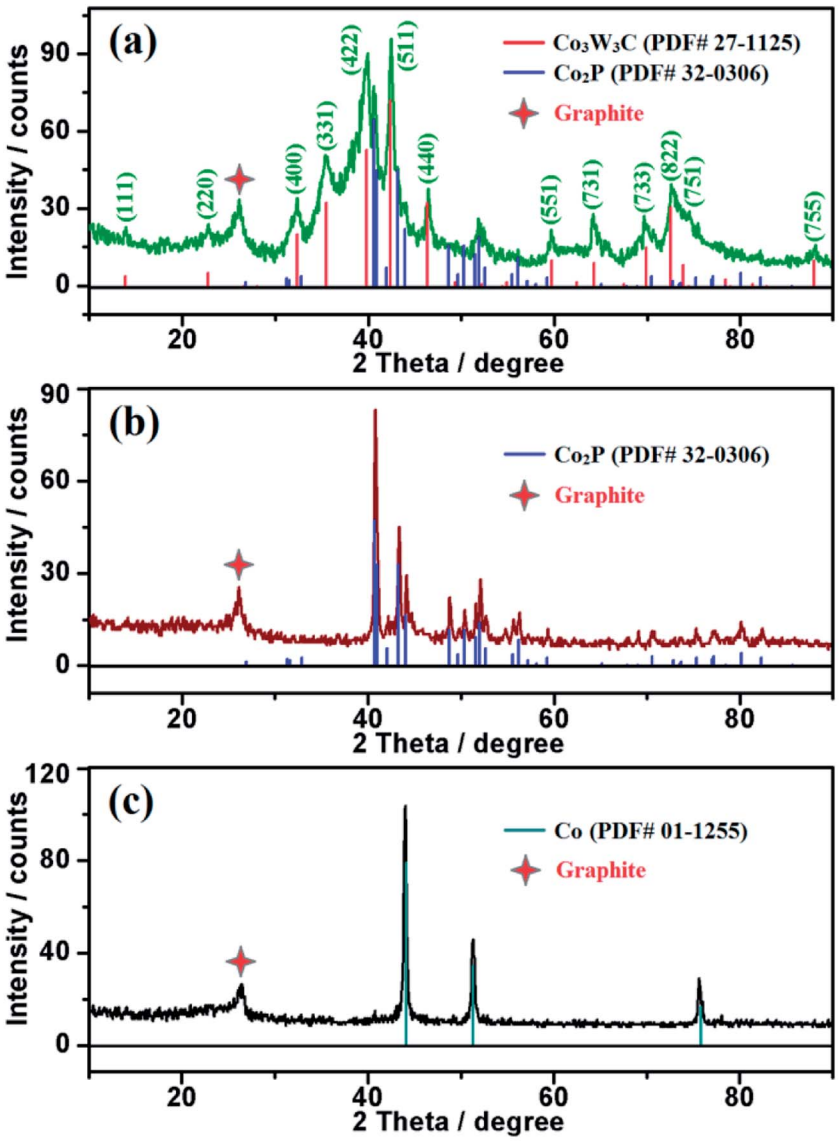

Fig. 1 XRD (a) Co_3W_3C/NPG (containing Co_2P), (b) NPG (containing Co_2P) and (c) NG (containing Co).

with underlying catalytic active sites (*e.g.* Co/N/P/C component) by the creation of N and P co-doped graphitic structures.

In order to analyze the carbide loading on the NPG support, the TGA analysis for the Co_3W_3C/NPG sample was further implemented in oxygen environment from 30 °C to 700 °C. From the TGA curve in Fig. 5, it can be seen that the sample has a small mass decrease between 30 °C and 100 °C (corresponding to the process of water losing) and a steady process between 100 °C and 350 °C. Afterwards, a fast mass decrease between 350 °C and 420 °C (corresponding to the process of carbon burning) can be observed. Obviously, the carbon content of Co_3W_3C/NPG sample can be calculated to be 39.8%, in other words, the carbide loading on the NPG support is 60.2%. In addition, the slight mass increase between 420 °C and 550 °C may be related to the phase transformation from carbide to oxide.

Relative to traditional method for synthesis of non-noble-metal catalyst, which requires laborious blending of Me precursors and nitrogen-/carbon precursors,[3,4] our strategy employs a convenient and effective procedure by introducing an amidogen-functionalized ion-exchange resin as the initial precursor, in which the amidogen group acts as nitrogen

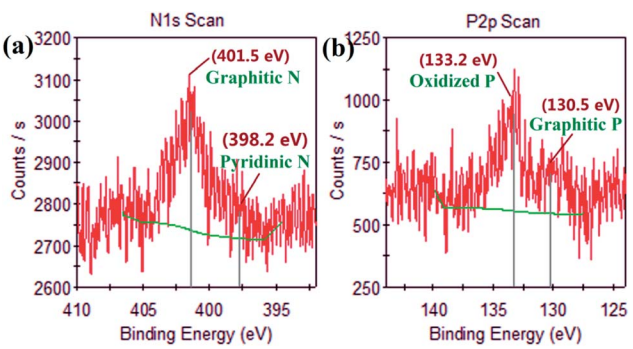

Fig. 2 (a) N1s and (b) P2p XPS spectrum of Co_3W_3C/NPG.

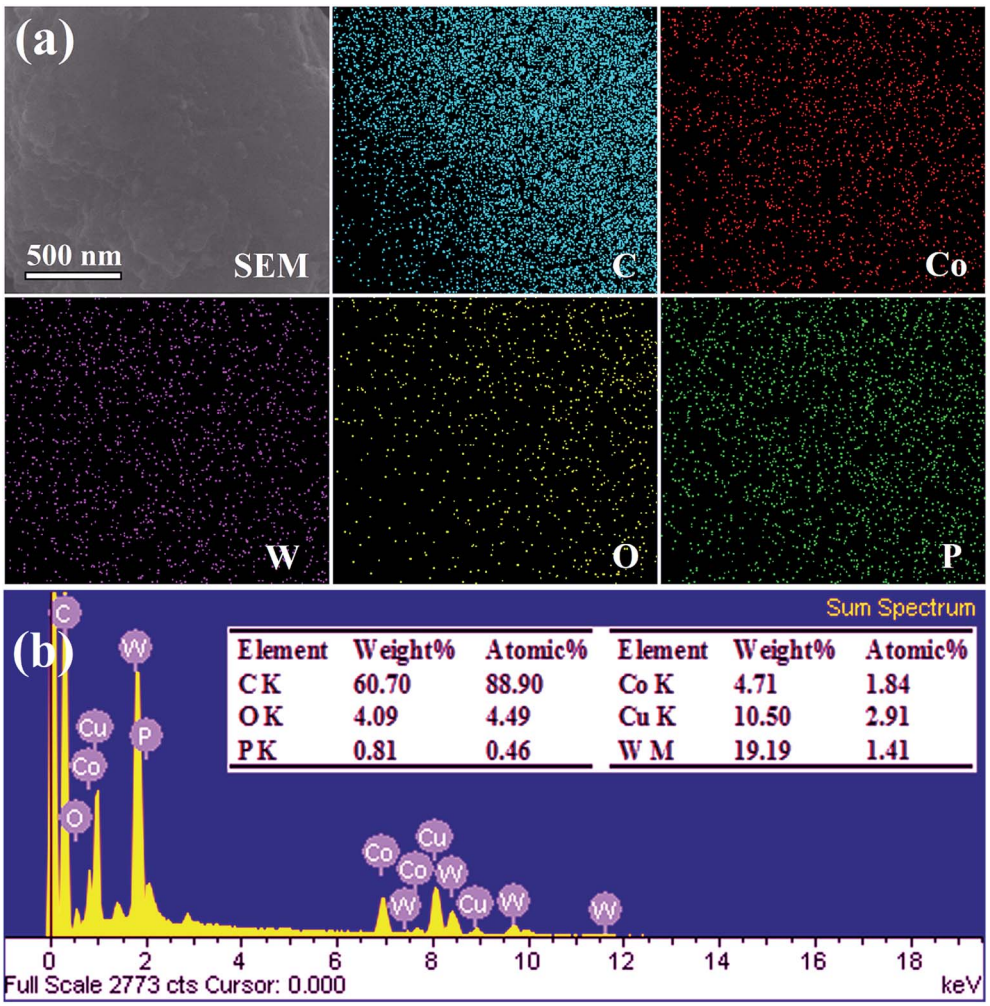

Fig. 3 SEM-EDS analysis of the Co_3W_3C/NPG: (a) SEM-EDS element mapping images and (b) EDS spectroscopy (the inset shows the element content).

sources and resin acts as carbon sources. The preparation procedures include the ion exchange with targeted ions (Co, W and P contained anions) followed by the heat treatment under inert atmosphere. Our ion exchange-assisted strategy can facilitate the synthesis of multi-component nanostructures, in which the targeted ions can be evenly localized within the precursor owing to its efficient ion-exchange role.[6]

To assess their ORR catalytic performances of diverse non-noble-metal catalysts, we performed rotating ring-disk electrode (RRDE) measurements in 0.1 M $HClO_4$ aqueous solution to achieve their ORR activity and stability (see Fig. 6). Fig. 6 (a) shows the ORR curves of various samples (Vulcan XC-72, NG, NPG and Co_3W_3C/NPG). For PEMFCs, an oxygen cathode with high potential and large current is essential to ensure the high cell working voltage and high energy conversion efficiency. Compared with Vulcan XC-72, the NPG sample shows a high on-set potential (0.84 V) and large limiting current (-4.5 mA cm^{-2}). Meaningfully, the NPG sample shows a higher on-set potential (0.89 V) and a larger limiting current (-5.0 mA cm^{-2}) than the NG sample. The results suggest that the N and P co-doped graphite (Co/N/P/C) is a more active non-noble-metal catalyst than the single N-doped graphite (Co/N/C) in acidic electrolyte. The half-wave potential ($E_{1/2}$), a potential at which the current is a half of the limiting current, has been widely used for estimate the ORR performance. Remarkably, the predominant ORR activity for the Co_3W_3C/NPG has been gleaned from its high onset potential (0.92 V), large limiting current (-5.3 mA cm^{-2}) and especially high half-wave potential ($E_{1/2}$ = 0.79 V). It is noted that the Co_3W_3C/NPG sample has an $E_{1/2}$ that is 60 and 160 mV higher than that of NPG and NG samples, respectively. The specific activities at 0.8 V of these catalysts are 0.20, 1.35 and 4.54 mA cm^{-2} for NG, NPG and Co_3W_3C/NPG, respectively (Fig. 6(b)). It is obvious that more than 6 times enhancement in activity was achieved by introducing phosphorus, and that is over 20 times when the intervention of Co_3W_3C component. In addition, the durability of the Co_3W_3C/NPG and NPG catalysts have been tested by cyclic voltammogram (CV) cycling between 0.0 and 1.1 V at 50 mV s^{-1} in O_2-saturated 0.1 M $HClO_4$ solution. After 8000 continuous cycles, the $E_{1/2}$ of ORR curves exhibited a small negative shift of 5 mV for Co_3W_3C/NPG catalyst, while

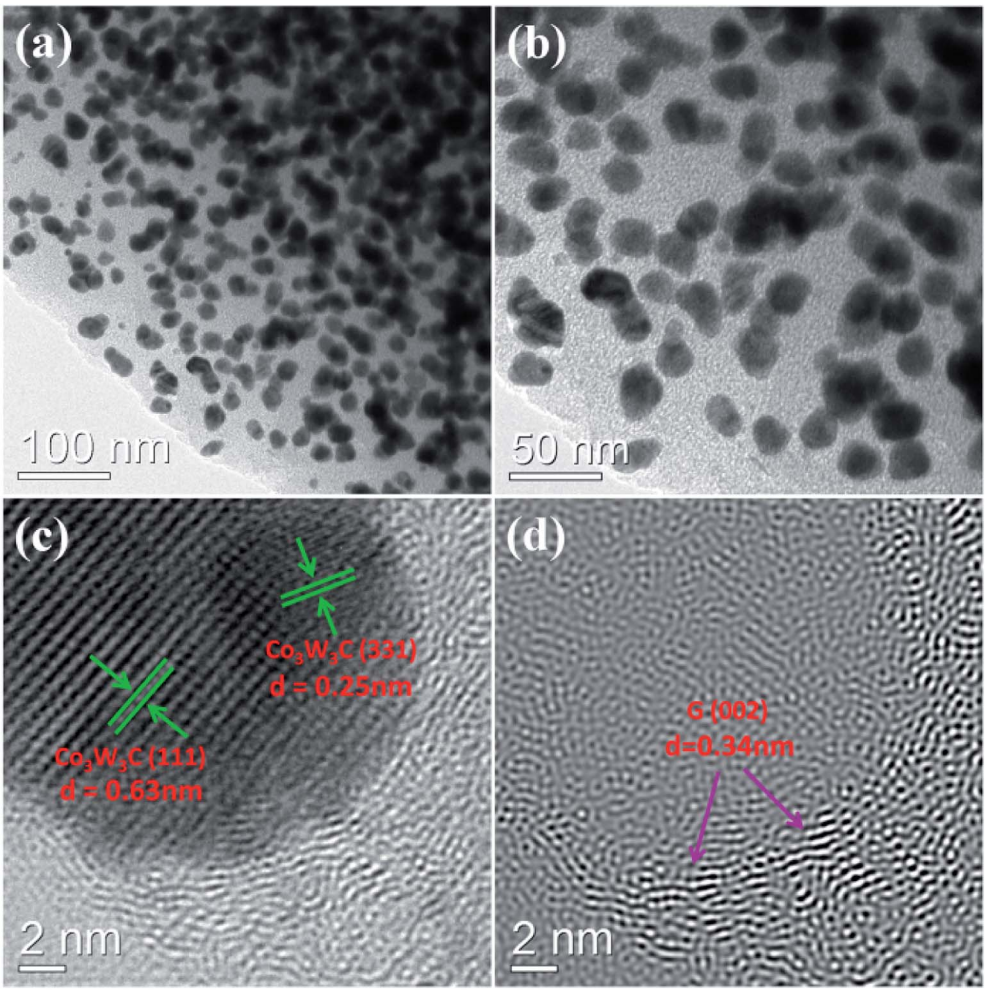

Fig. 4 TEM images of the Co_3W_3C/NPG: (a) and (b) low-magnification images, (c) a high-resolution image and (d) graphite (002)-oriented Inverse Fourier Transform (IFT) image based on image (c).

that is 30 mV for NPG catalyst (Fig. 6(c)). A high activity retention of 97% is achieved for Co_3W_3C/NPG catalyst which is much higher than that 58% of NPG catalyst (Fig. 6(d)), making it one of promising non-noble-metal catalysts for acidic oxygen reduction reaction.[5]

To show further insight into the evidence and mechanism of the excellent performances, the corresponding CV curves and ring currents Co_3W_3C/NPG and NPG catalysts before and after 8000 CV cycles are shown in Fig. 7 and Fig. 8, respectively. The CV curves in Fig. 7 reveal that Co_3W_3C/NPG catalyst behaves a pronounced cathodic ORR peak at 0.75 V, while that is only 0.66 V for NPG catalyst in O_2-saturated 0.1 M $HClO_4$ solution. The decrease of ORR peak is limited for Co_3W_3C/NPG catalyst, relative to the distinct decrease of NPG catalyst. One of the problems plaguing non-noble-metal catalysts is the oxidation by peroxide intermediates, leading to easily catalyst deactivation.[12] Therefore, low peroxide yield is an indispensable index for the highly active and stable electrocatalyst. Based on the ring currents in Fig. 8(a), the calculated peroxide yields at 0.6 V (Fig. 8(b)) are 1.15% and 1.39% for Co_3W_3C/NPG before and after 8000 CV cycles, respectively. The two values are much lower than these of NPG (0.6 V: 4.67% and 10.36% before and after 8000 CV cycles). The above results are well responding for the excellent catalytic performances of the Co_3W_3C/NPG catalyst. In addition, the electron transfer number (n) was calculated

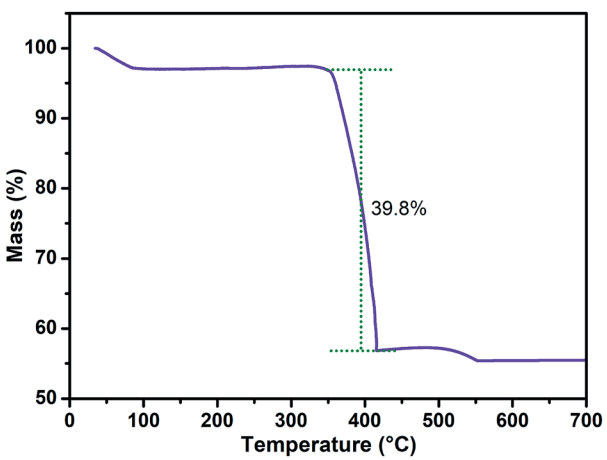

Fig. 5 TGA analysis of the Co_3W_3C/NPG.

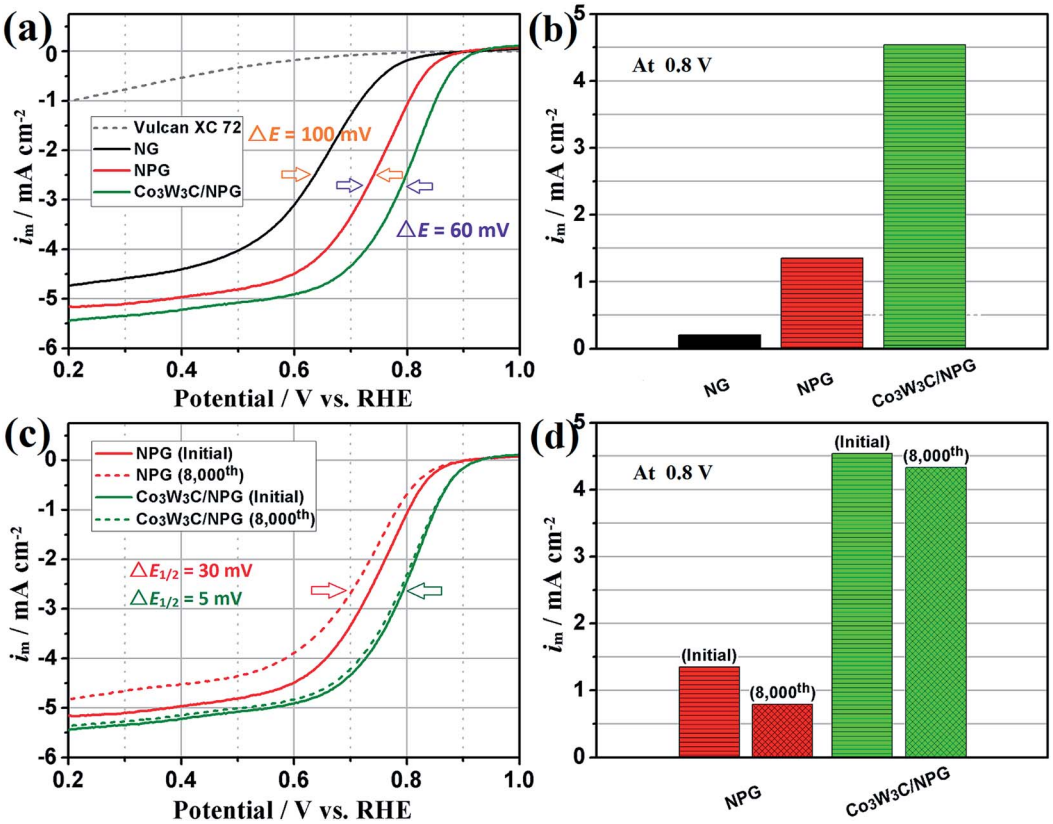

Fig. 6 (a) ORR curves and (b) specific activities of diverse non-noble-metal catalysts; (c) ORR curves and (d) specific activities the NPG and Co_3W_3C/NPG before and after 8000 CV cycles. The ORR were performed in O_2-saturated 0.1 M $HClO_4$ solution, at a rotation speed of 1600 rpm and a scan rate of 5 mV s^{-1} under 30 °C.

to be 3.97 at 0.6 V (Fig. 8 (c)) from the ring currents, suggesting the Co_3W_3C/NPG catalyst has a 4e oxygen reduction process.

Because all these samples have equivalent nitrogen doping and the same Co addition, the promoted effects from phosphorus and carbide should be the fundamental reason for the improvement in catalytic performances for Co_3W_3C/NPG catalyst. For one thing, the electronic effects of N and P co-doping of graphite could play an important role in ORR. Note that Me–N species is believed to be ORR-active sites in Fe/N/C or Co/N/C catalysts prepared by the heat treatment.[4] Phosphorus has the same number of valence electrons as nitrogen and often shows similar chemical properties.[9] Thus the electronic effects of Co/N/P/C catalysts should be more prominent than Co/N/C catalysts. At the same time, the bimetallic carbide Co_3W_3C as a synergistic component could afford a stronger coupling between the Co species and graphitic structures in Co_3W_3C/NPG (Co/N/P/C) than in NG (Co/N/C), thus contributing

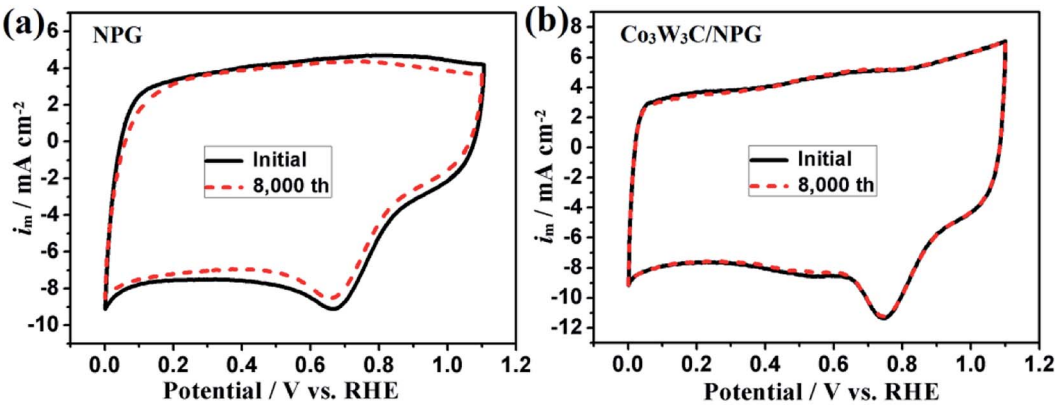

Fig. 7 CV curves of the NPG and Co_3W_3C/NPG at 50 mV s^{-1} in O_2-saturated 0.1 M $HClO_4$ solution before and after 8000 CV cycles.

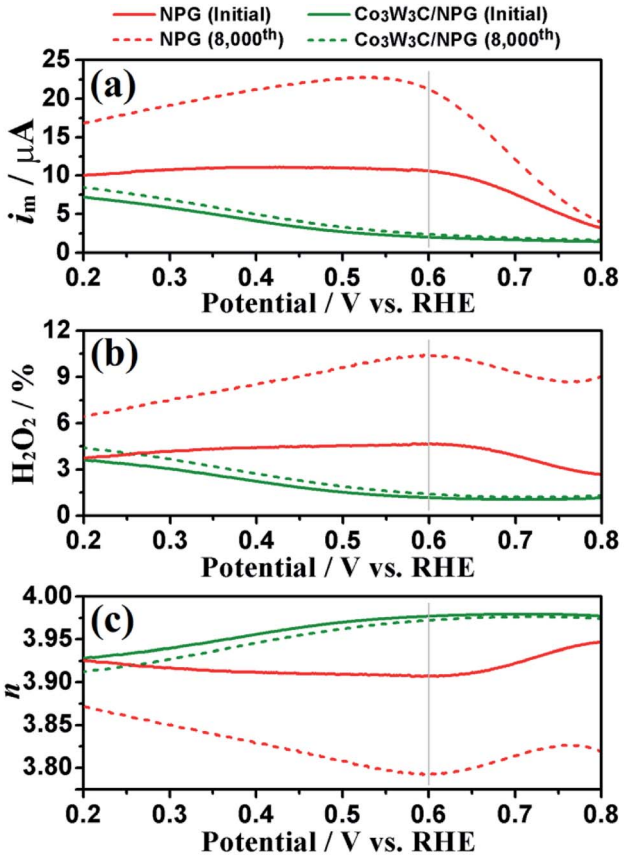

Fig. 8 (a) Ring current, (b) peroxide (H_2O_2) percentage, (c) electron transfer number (n) of the NPG and Co_3W_3C/NPG before and after 8000 CV cycles.

higher catalytic activity and stability for present non-noble-metal catalysts.

Recently, Shen and co-workers have proposed several bimetallic carbides (*e.g.* $Co_6Mo_6C_2$,[13] Fe_2MoC[14] and Co_3W_3C[15]) at low-platinum and non-platinum electrocatalysts, which represented excellent ORR catalytic activity. For example, low-platinum catalyst prepared by loading a small amount of Pt on $Co_6Mo_6C_2$/GC showed much higher ORR activity and stability in comparison with commercial Pt/C in acidic solution.[13] The Pd supported on Fe_2MoC/GC[14] or Co_3W_3C/GC[15] as non-platinum electrocatalysts also shows superior ORR activity and stability to commercial Pt/C in acidic solution. More importantly, as acidic non-noble-metal catalysts, the ORR catalytic activity of these bimetallic carbides has been improved gradually ($Co_6Mo_6C_2$/GC with a 0.68 V onset potential[13] and Fe_2MoC/GC with a 0.78 V onset potential[14]), owing to the multi-metal components and the favorable crystal structures. It is worth mentioning that the onset potential of Co_3W_3C/NPG has been increased to 0.92 V in this work (with a high half-wave potential of 0.79 V), which might be a considerable improvement in ORR catalytic activity. The above researches provide a theoretical basis for the design of a new type of bimetallic carbide-based non-noble-metal electrocatalysts.

Previously, Dai and co-workers clarified that the nitrogen doped graphene/Co_3O_4 composite possessed ultrahigh catalytic activity in alkaline solution, due to the electronic coupling synergistic effect between metal species nitrogen doped graphene.[16] The source of high activity of this composite material is the change of the chemical bond of the interface atoms of N, C, O and Co during the two-component coupling process. Based on this, the intrinsic activity of Co_3W_3C/NPG in acidic solution could be also connected with the optimal electronic and geometric structures of the interface atoms of N, P, C, W and Co. The specific mechanism needs further study. In general, the atomic level regulation of active component is very important for the design of high-performance ORR catalyst. More recently, Wu and co-workers reported an ultrahigh-performance nitrogen-coordinated single Co atom catalyst for ORR in challenging acidic media (*e.g.*, half-wave potential of 0.80 V *vs.* RHE).[17] An atomically Co site dispersed catalyst with optimal chemical and structural properties has been achieved by investigating effects of Co doping contents and thermal activation temperature. The same effects were confirmed for the design of single atomic iron catalysts,[18,19] which will be a promising development direction for advanced non-noble-metal electrocatalysts.

4. Conclusions

In summary, we have developed a novel bimetallic carbide enhanced nitrogen/phosphor co-doped graphite nanocomposite (Co_3W_3C/NPG) by an effective ion exchange-assisted heat treatment strategy. The Co_3W_3C/NPG catalyst is demonstrated to be a high-performance catalyst for oxygen reduction reaction (ORR). On account of the synergetic effects of bimetallic carbide (Co_3W_3C), the Co_3W_3C/NPG catalyst showed much higher activity and stability than the NPG catalyst in 0.1 M $HClO_4$ aqueous solution, making it a promising non-noble-metal catalyst for acidic ORR.

Conflicts of interest

There are no conflicts to declare.

Acknowledgements

Financial support by the National Natural Science Foundation of China (21606052), Provincial Natural Science Foundation of Guangdong (2017A030313049), Excellent Young Teacher Training Project of Guangdong Province Education Department (YQ2015115), are gratefully acknowledged.

References

1 M. Shao, Q. Chang, J. Dodelet and R. Chenitz, Recent advances in electrocatalysts for oxygen reduction reaction, *Chem. Rev.*, 2016, **116**, 3594–3657.
2 D. He, D. He, J. Wang, Y. Lin, P. Yin, X. Hong, Y. Wu and Y. Li, Ultrathin icosahedral Pt-enriched nanocage with excellent oxygen reduction reaction activity, *J. Am. Chem. Soc.*, 2016, **138**, 1494–1497.

3 G. Wu and P. Zelenay, Nanostructured nonprecious metal catalysts for oxygen reduction reaction, *Acc. Chem. Res.*, 2013, **46**, 1878–1889.
4 G. Wu, K. L. More, C. M. Johnston and P. Zelenay, High-performance electrocatalysts for oxygen reduction derived from polyaniline, iron, and cobalt, *Science*, 2011, **332**, 443–447.
5 Y. Li, W. Zhou, H. Wang, L. Xie, Y. Liang, F. Wei, J. Idrobo, S. Pennycook and H. Dai, An oxygen reduction electrocatalyst based on carbon nanotube-graphene complexes, *Nat. Nanotechnol.*, 2012, **7**, 394–400.
6 Z. Li, Z. Liu, B. Li, Z. Liu, D. Li, H. Wang and Q. Li, Hollow hemisphere-shaped macroporous graphene/tungsten carbide/platinum nanocomposite as an efficient electrocatalyst for the oxygen reduction reaction, *Electrochim. Acta*, 2016, **221**, 31–40.
7 E. Antolinia and E. Gonzalez, Tungsten-based materials for fuel cell applications, *Appl. Catal., B*, 2010, **96**, 245–266.
8 G. Cui, P. Shen, H. Meng, J. Zhao and G. Wu, Tungsten carbide as supports for Pt electrocatalysts with improved CO tolerance in methanol oxidation, *J. Power Sources*, 2011, **196**, 6125–6130.
9 Z. Liu, F. Peng, H. Wang, H. Yu, W. Zheng and J. Yang, Phosphorus-doped graphite layers with high electrocatalytic activity for the O_2 reduction in an alkaline medium, *Angew. Chem.*, 2011, **123**, 3315–3319.
10 J. Zhang, L. Qu, G. Shi, J. Liu, J. Chen and L. Dai, N, P-codoped carbon networks as efficient metal-free bifunctional catalysts for oxygen reduction and hydrogen evolution reactions, *Angew. Chem.*, 2016, **128**, 2270–2274.
11 L. Lin, Q. Zhu and A. W. Xu, Noble-metal-free Fe–N/C catalyst for highly efficient oxygen reduction reaction under both alkaline and acidic conditions, *J. Am. Chem. Soc.*, 2014, **136**, 11027–11033.
12 Y. Liang, H. Wang, P. Diao, W. Chang, G. Hong, Y. Li, M. Gong, L. Xie, J. Zhou, J. Wang, T. Regier, F. Wei and H. Dai, Oxygen reduction electrocatalyst based on strongly coupled cobalt oxide nanocrystals and carbon nanotubes, *J. Am. Chem. Soc.*, 2012, **134**, 15849–15857.
13 X. Ma, H. Meng, M. Cai and P. Shen, Bimetallic carbide nanocomposite enhanced Pt catalyst with high activity and stability for the oxygen reduction reaction, *J. Am. Chem. Soc.*, 2012, **134**, 1954–1957.
14 Z. Yan, M. Zhang, J. Xie, J. Zhu and P. Shen, A bimetallic carbide Fe_2MoC promoted Pd electrocatalyst with performance superior to Pt/C towards the oxygen reduction reaction in acidic media, *Appl. Catal., B*, 2015, **165**, 636–641.
15 Z. Li, S. Ji, B. Pollet and P. Shen, A Co_3W_3C promoted Pd catalyst exhibiting competitive performance over Pt/C catalysts towards the oxygen reduction reaction, *Chem. Commun.*, 2014, **50**, 566–568.
16 Y. Liang, Y. Li, H. Wang, J. Zhou, J. Wang, T. Regier and H. Dai, Co_3O_4 nanocrystals on graphene as a synergistic catalyst for oxygen reduction reaction, *Nat. Mater.*, 2011, **10**, 780–786.
17 X. Wang, D. Cullen, Y. Pan, S. Hwang, M. Wang, Z. Feng, J. Wang, M. Engelhard, H. Zhang, Y. He, Y. Shao, D. Su, K. More, J. Spendelow and G. Wu, Nitrogen-coordinated single cobalt atom catalysts for oxygen reduction in proton exchange membrane fuel cells, *Adv. Mater.*, 2018, **30**, 1706758.
18 H. Zhang, S. Hwang, M. Wang, Z. Feng, S. Karakalos, L. Luo, Z. Qiao, X. Xie, C. Wang, D. Su, Y. Shao and G. Wu, Single atomic iron catalysts for oxygen reduction in acidic media: particle size control and thermal activation, *J. Am. Chem. Soc.*, 2017, **139**, 14143–14149.
19 Z. Qiao, H. Zhang, S. Karakalos, S. Hwang, J. Xue, M. Chen, D. Su and G. Wu, 3D polymer hydrogel for high-performance atomic iron-rich catalysts for oxygen reduction in acidic media, *Appl. Catal., B*, 2017, **219**, 629–639.